

Application of thermal-derivative analysis to study phase transformation in AlSi₇Mg alloy with different iron content

Jarosław Piatkowski¹, Leszek Chowaniec², Tomasz Matula³

Silesian University of Technology^{1,3}, Superior Industries Production Poland Sp. z o.o.², Poland

E-mail: jaroslaw.piatkowski@polsl.pl, leszek.chowaniec@pro.onet.pl, tomasz.matula@polsl.pl

Abstract: Using an increasing share of aluminum scrap (production and post-production) requires paying special attention to its impurities. Gaseous inclusions (e.g., hydrides) can be removed from the liquid alloy by refining, but the situation is worse with metallic impurities. In Al-Si alloys, one of the worst is iron, which goes into solution due to its low solubility in the solid state, at a content of over 0.4wt.%, it crystallizes in morphologically unfavorable phases, which worsen the functional properties and increase the porosity of aluminum alloys, limiting their use. The crystallization of these phases causes thermal effects that various methods can record. The paper presents studies of phase transformation, especially iron phases, using thermal-derivative analysis occurring in the AlSi₇Mg alloy with different iron content. The studies were performed on Crystaldigraph NT3-8K coupled with the MLab program. It was found that the most unfavorable phase is β -Al₅FeSi, which crystallizes preeutectic (and mainly primary crystallize) dimensions of up to 1000 μ m, causing the formation of shrinkage porosities.

KEYWORDS: AL-SI CAST ALLOYS; THERMAL ANALYSIS; PHASE TRANSFORMATION; CRYSTALLIZATION; POROSITY

1. Introduction

Analysis of thermodynamic processes is proper when it is possible to record their kinetics. In industrial settings, temperature is the parameter that can be most easily controlled and determines the form of the microstructure and the physicochemical properties occurring in the material. One of the methods of the time course of change of these properties as a function of temperature is thermal analysis (TA) [1-3]. Among its many variations, e.g., thermogravimetric analysis (TGA) [4, 5], thermodilatometric analysis (TDA) [6], thermomechanical analysis (TMA) [7] or differential scanning calorimetry (DSC) [8, 9], thermal-derivative analysis (TDA) has found wide application in both laboratory and industrial research [10-12]. ATD analysis is a method that uses the visual effects of phase transformations occurring in metal alloys (usually during the transition from the liquid to the solid state), accompanied by a change in energy. As the sample cools, its temperature is lowered by the release of heat, a characteristic feature of the alloy under study and the transformations taking place in it. Due to the ease of measuring temperature, the ATD method is widely used, for example, in metallurgy, making it possible to quickly obtain much information about the alloy under study [13-16].

Such great interest in the ATD method is due to its versatile application for, among other things:

- nucleation analysis and determination of the degree of overcooling of the alloy ΔT . It can be used, for example, to assess the correctness of the modification process incident - the beginning of the cooling curve,
- indicative prediction of the chemical and structural composition of the alloy - the middle range of the crystallization curve (from T_{liq} to T_{sol}),
- indicative assessment of the alloy's purity and the presence of impurities, inclusions, and gases in it - the final section of the crystallization curve. Impurities cause the formation of low-melting eutectics, which affect a significant increase in crystallization time,
- determination of the amount of heat of crystallization of alloying elements and eutectics - the entire crystallization curve,
- evaluation of phase transformations due to the separation of intermetallic phases (separate or as a component of eutectics).

In particular, the last capability of the ATD method helps determine the range of crystallization temperatures of alloying constituents, for example, in alloys where crystallization of phases that negatively affect functional properties is possible. This mainly concerns iron phases of unfavorable morphology in aluminum alloys due to the increased proportion of circulating scrap as a feedstock component.

Studies [20-22] indicate that the iron contained in Al-Si alloys, as a result of different heat removal conditions and chemical

composition, can crystallize in the form of four phases with different morphologies:

1. β -Al₅FeSi, also referred to as Al₉Fe₂Si in Group 6XX.X (Al-Mg-Si) alloys,
2. α -Al₈Fe₂Si (or α -Al₁₂Fe₃Si₂), which under thermodynamic equilibrium conditions has a hexagonal structure and is stable only in Al-Si-Fe alloys with high charge purity,
3. δ -Al₄FeSi₂ present in Al-Si alloys with more than 18 wt. % Si, and
4. γ -Al₃FeSi present at contents of more than 4 wt. % Fe and more than 16 wt. % Si.

However, the problem arises when the iron content in Al-Si alloys exceeds 0.4wt.% (for gravity castings), resulting in the crystallization of the β -Al₅FeSi phase (which has a lamellar and needle-like structure). As reported in the literature [17, 18], such a structure causes the propagation of microcracks and stress concentration, which increases the brittleness of castings, makes them more difficult to machine, reduces mechanical properties, and increases porosity. Therefore, it seems reasonable to research evaluating the crystallization of Al-Si alloys with higher iron content and analyzing the associated phase transformations. This problem is particularly relevant as the share of circulating scrap in producing Al-Si(Fe) alloy castings needs to be increased for economic and environmental reasons.

2. Purpose and scope of the research

The study aimed to analyze the crystallization process of an AlSi₇Mg alloy with increasing iron content (from 0.4 to 2.0wt.%, in 0.2% increments) and its effect on microstructure and porosity.

To realize the stated purpose of the work, the scope of the research included:

- execution of melts according to the established experimental plan (Fig.1),
- chemical composition studies,
- analysis of crystallization by ATD method: recording the cooling curve and its first derivative,
- evaluation of microstructure change and porosity of AlSi₇Mg alloy with different iron content.

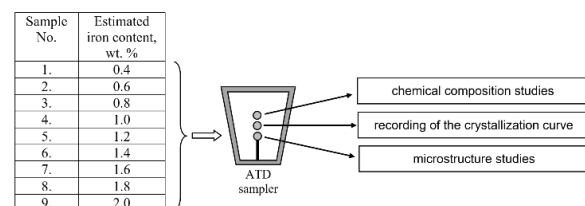


Fig. 1. Research plan for the AlSi₇Mg alloy with increasing iron content.

3. Research material and methodology

The material for the study was AlSi7Mg alloy. The choice of the alloy was dictated by its wide application, both for gravity castings and pressure castings, such as rims. AlFe20 master alloy (as a substitute for scrap iron) was added to the alloy in such quantities as to achieve the assumed content of 0.4 to 2.0wt.% Fe (Fig.1). Any magnesium deficiencies were supplemented with AlMg10 master alloy (10wt.% Mg). The alloys were smelted in a Balzers VSG02/631 electric vacuum furnace (Balzers & Co GmbH, Germany). The alloys were modified with AlSr10 master alloy and refined with Rafglin-3. After reaching a temperature of about 760°C, it was cast into a standard QC-4080 Heraeus Electro-Nite sampler (Seekirchen, Austria) with a capacity of 130 cm³. The solidification temperature (T) was recorded using a NiCr-NiAl thermocouple (type K) placed on the axis of the sampler. Thermal analysis was carried out with a Crystaldigraph NT3-8K temperature recorder using MLab software (Gliwice, Poland). This set meets the requirements of both EN61010 and EN60584 for temperature measurement. The cooling curve $T=f(\tau)$ and its first derivative in time $dT/d\tau=f'(\tau)$ were recorded. For each measurement of the cooling curve, the same volume of alloy, the same coefficients for "smoothing" the first derivative, and similar melting, casting, and ambient conditions were used. From the middle part of the cross-section of the QC-4080 sampler ingot (at the temperature measurement point), samples were taken for metallographic studies performed on a MeF-2 Reichert light microscope (Wien, Austria). X-ray microanalysis was conducted on a Hitachi S-4200 scanning microscope (Tokyo, Japan) with an EDS energy dispersive X-ray spectrometer using a Thermo Noran system (System Six) equipped with a SE and BSE electron detector. X-ray studies were performed with a Philips X'Pert diffractometer, using a $\lambda_{CuK\alpha} - 1.54178 \text{ \AA}$ lamp supplied with 30 mA at 40 kV. The registration was made using the "step-scan" method with a step of 0.04° and a counting time of 10 seconds, in the 2 θ angle range from 20° to 140°. The gap on the incident beam was 1°, and on the deflected beam was 2°.

4. Research results and their analysis

4.1. Chemical composition test results

The results of the chemical composition of AlSi7Mg alloy with increasing iron content are shown in Table 1.

Table 1. Results of the chemical composition of AlSi7Mg (Al - balance) alloy.^{1,2}

Sample No.	Element content, wt. %										
	Si	Fe	Mg	Cu	Mn	Ni	Sn	Zn	Pb	Ti	
1.	6.94	0.39	0.55	0.18	0.28	0.09	≤0.01	≤0.08	≤0.11	0.12	
2.	6.93	0.61	0.54	0.17	0.32	0.13	≤0.01	≤0.09	≤0.10	0.13	
3.	7.11	0.80	0.60	0.16	0.29	0.06	≤0.02	≤0.11	≤0.09	0.13	
4.	7.02	0.97	0.52	0.11	0.31	0.09	≤0.03	≤0.06	≤0.10	0.12	
5.	7.41	1.16	0.58	0.16	0.27	0.11	≤0.02	≤0.11	≤0.11	0.18	
6.	6.95	1.39	0.61	0.17	0.24	0.11	≤0.02	≤0.09	≤0.10	0.17	
7.	7.17	1.59	0.58	0.15	0.30	0.08	≤0.03	≤0.11	≤0.09	0.20	
8.	7.26	1.78	0.52	0.16	0.30	0.08	≤0.02	≤0.07	≤0.10	0.15	
9.	7.22	1.94	0.55	0.19	0.27	1.12	≤0.02	≤0.11	≤0.08	0.18	

¹ – averaged results from 6 measurements, after excluding the two extreme ones,

² – the sum of other elements (Na) and impurities (Ca; K) in the AlSi7Mg alloy is below 0.05.

Analyzing the results of the chemical composition of the AlSi7Mg alloy (Table 1), it can be concluded that despite the increasing iron content, the proportion of other elements has not changed and is within the limits of a typical AlSi7Mg alloy.

4.2. Results of thermal analysis using the ATD method

Representative ATD plots of AlSi7Mg alloy with different iron contents are shown in Figure 2.

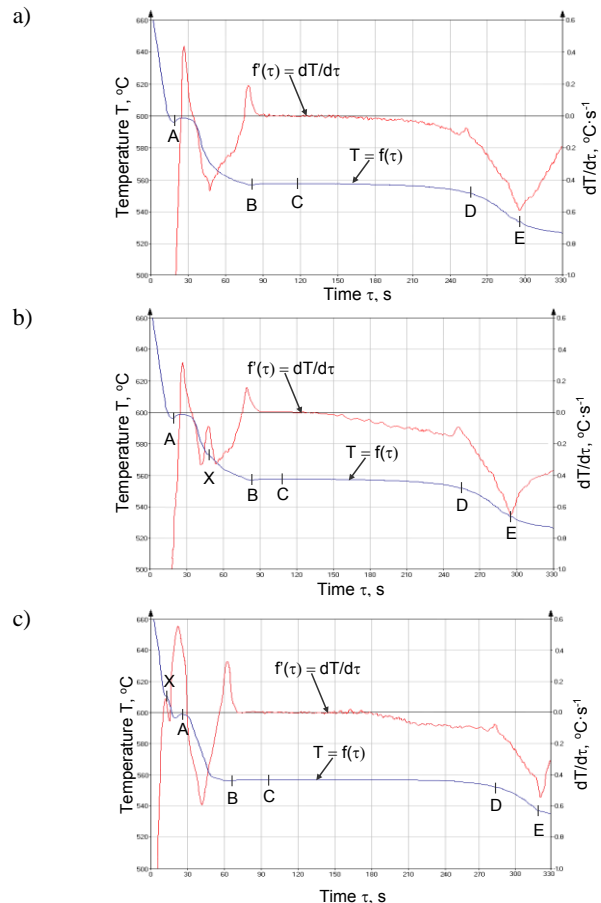


Fig. 2. Crystallization curves of AlSi7Mg alloy with different iron content: a) up to 0.49wt.%; b) from about 0.5 to 0.9wt.%; c) from about 0.91 to 1.5wt.%. The symbols in Figure 2 stand for:

The symbols in Figure 2 stand for:

- $T=f(\tau)$ - the curve of temperature change T at time τ , - the so-called TA (Temperature Analysis) curve,
- $dT/d\tau=f'(\tau)$ - the first derivative of the temperature change over time - the so-called ATD (Analysis Temperature Derivative) curve,
- point A - temperature of onset of crystallization of dendrites of solid solution $\alpha(\text{Al}) - T_{\alpha(\text{Al})}(T_{\text{liq}})$, °C,
- A-B - range of crystallization of dendrites of solid solution $\alpha(\text{Al})$, °C,
- point B - minimum temperature (onset) of crystallization of eutectic $\alpha(\text{Al})+\beta(\text{Si})$, - $T_{\text{Emin}(\alpha+\beta)}$, °C,
- point C - average crystallization temperature of the $\alpha(\text{Al})+\beta(\text{Si})$, - $T_{\text{E}(\alpha+\beta)}$, °C,
- point X - crystallization temperature of iron-rich intermetallic phases - $T_{\text{E(Fe)}}$, °C,
- point D - crystallization temperature of magnesium-rich intermetallic phases - $T_{\text{E(Mg)}}$, °C,
- point E - temperature of the end of crystallization of EN AC-AlSi7Mg alloy (T_{sol}), °C.

Table 2 summarizes the average characteristic crystallization temperatures of AlSi7Mg alloy obtained from the ATD method (rounded to integer) for different iron contents. Based on ATD studies, the cooling curve of AlSi7Mg alloy is up to about 0.49wt.% Fe content was found to be typical of Al-Si-Mg alloys with sub-eutectic composition, i.e., dendrites of the solid solution $\alpha(\text{Al})$ -at T_{liq} are formed first, followed by crystallization of the eutectics $\alpha(\text{Al})+\beta(\text{Si})$ and $\alpha(\text{Al})+(\text{Mg}_2\text{Si})+\beta(\text{Si})$, at about 0.5 to about 0.9wt.% Fe, an exothermic effect from crystallization of iron-rich phases was found. It occurs in the temperature range from about 574°C to about 590°C, which is before the crystallization of the $\alpha(\text{Al})+\beta(\text{Si})$ eutectic (about 558°C) and the triple eutectic containing the Mg_2Si phase (about 550°C). Crystallization of these eutectics continues to the temperature of T_{sol} . (from about 530 to 520°C). Iron content in the AlSi7Mg alloy up to more than 0.9wt.% causes

primary crystallization of the iron phases (before crystallization of the dendrites of the solid solution α), accompanied by an exothermic effect at temperatures above 590°C. Further increasing the proportion of iron results in an even more significant increase in $T_{E(Fe)}$ temperatures to as high as 640°C for 2.0wt.% Fe content. Increasing the proportion of iron and the resulting increase in the $T_{E(Fe)}$ temperature value changes the microstructure of the AlSi7Mg alloy.

Table 2. Characteristic crystallization temperatures of AlSi7Mg alloy from ATD analysis¹.

Sample No.	Name of alloy and share of iron, wt. %	Characteristic crystallization temperatures, °C					
		A T_{liq}	B $T_{Emin(\alpha+\beta)}$	C $T_{E(\alpha+\beta)}$	X $T_{E(Fe)}$	D $T_{E(Mg)}$	E T_{sol}
1.	AlSi7Mg+0.4	590	555	558	---	551	532
2.	AlSi7Mg+0.6	590	556	558	---	550	530
3.	AlSi7Mg+0.8	592	555	557	574	551	530
4.	AlSi7Mg+1.0	595	556	559	579	551	525
5.	AlSi7Mg+1.2	596	554	557	591	551	522
6.	AlSi7Mg+1.4	600	556	557	619	550	522
7.	AlSi7Mg+1.6	603	556	558	624	550	520
8.	AlSi7Mg+1.8	604	555	558	633	550	520
9.	AlSi7Mg+2.0	606	556	558	640	551	520

¹ – the symbols in the table are the same as in Figure 2.

4.3. Microstructure test results

Figure 3 shows representative microstructures of AlSi7Mg alloys with different iron contents. Figure 4 shows X-ray scattered energy spectra and micro-area chemical composition, and Figure 5 shows the X-ray diffractogram.

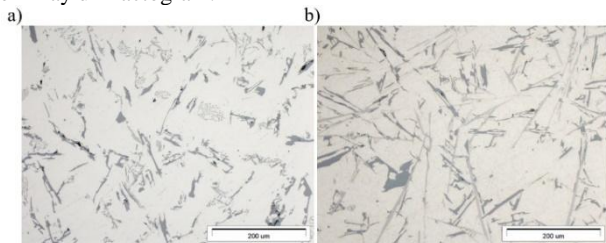


Fig. 3. Representative microstructures of AlSi7Mg alloy with different iron content: a) up to 0.49wt.%; b) from about 0.5 to 0.9wt. %.

The study of the microstructure of the AlSi7Mg alloy shows that, in addition to the traditional components, i.e., the dendrites of the $\alpha(Al)$ solid solution, the silicon crystals included in the $\alpha(Al)+\beta(Si)$ eutectic and the Mg_2Si phase included in the $\alpha(Al)+Mg_2Si+\beta(Si)$ eutectic, the $\beta-Al_5FeSi$ phase was identified. Its structure resembles a “slab” with sharp edges, which on the surface of the metallographic specimen is visible as a “needle-like” separation with pointed corners. The privileged direction of propagation to one side causes the $\beta-Al_5FeSi$ phase, especially at maximum iron content, to be often cracked [19].

It can be seen from Figure 6 that long precipitations of $\beta-Al_5FeSi$ phases (from 600 μm to even 1000 μm - at contents of more than 0.9wt.% Fe) are privileged sites for the formation of porosity, affecting the reduction of interdendritic permeability, thus blocking (inhibiting) the free flow of liquid melt during cooling. The moving crystallization front “does not keep up” with the filling with the liquid metal of the sites “closed” by $\beta-Fe$ phases, causing the formation of shrinkage pores in the vicinity of $\beta-Al_5FeSi$ phases. The presence of voids causes local stresses, which transform into micro- and macro-cracks during the casting operation. This is because igneous separations of $\beta-Fe$ phases oriented with the longer side perpendicular to the given load undergo decohesion, while those arranged in parallel - crack along their arms and undergo fragmentation. Thus, it is reasonable to believe that the $\beta-Al_5FeSi$ phases appear in the microstructure of the AlSi7Mg alloy after exceeding about 0.5wt.% Fe represents the nuclei of pores and/or shrinkage microcracks, increasing the porosity of the castings and reducing the feed capacity by reducing the flow of liquid melt between the branched dendrites of the $\alpha(Al)$ solid solution. This is in line with the view presented in studies [20, 21], which show that these voids are sites of microcrack initiation.

Observations of the microstructure of the AlSi7Mg alloy also revealed numerous clusters of shrinkage-type porosity, examples of which are shown in Figure 6.

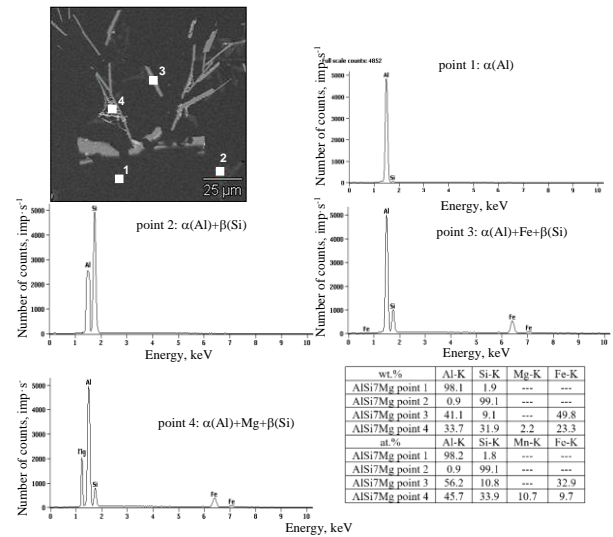


Fig. 4. Microstructure and scattered energy X-ray spectra and chemical composition in micro areas of AlSi7Mg alloy.

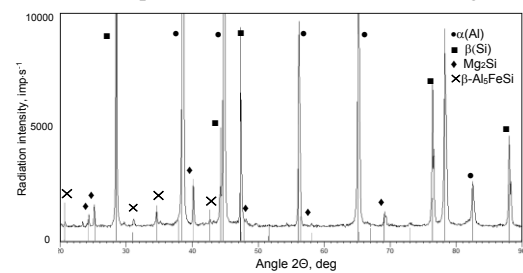


Fig. 5. XRD X-ray of AlSi7Mg alloy with about 0.9wt.% Fe.

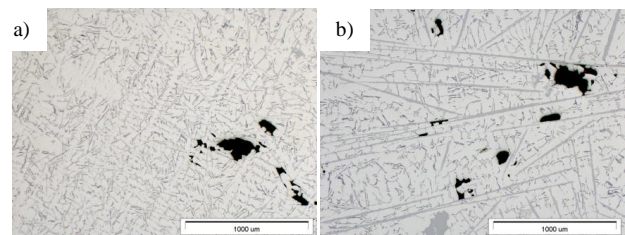


Fig. 6. Microstructure of AlSi7Mg alloy with different iron content: a) up to 0.49wt.%; b) from about 0.5 to 0.9wt. %.

5. Summary and conclusions

Based on ATD studies, it can be concluded that the crystallization of AlSi7Mg alloy with increasing iron content proceeds in the following stages:

- for contents up to about 0.45wt.% Fe:
 - Stage 1: start of the crystallization process of dendrites of the solid solution $\alpha(Al)$ - temperature T_{liq} .
 - Stage 2: nucleation and crystallization of the double eutectic $\alpha(Al)+\beta(Si)$ - temperature $T_{E(\alpha+\beta)}$.
 - Stage 3: nucleation and crystallization of multicomponent eutectics $\alpha(Al)+Al_xFe_ySi_z+\beta(Si)$ and triple $\alpha(Al)+Mg_2Si+\beta(Si)$ - $T_{E(Fe)}$ and $T_{E(Mg)}$ temperatures.
 - Stage 4: end of alloy crystallization process - T_{sol} temperature.
- for contents from about 0.46 to 0.9wt.% Fe:
 - Stage 1: start of solid solution dendrite crystallization $\alpha(Al)$ - T_{liq} .
 - Stage 2: nucleation and pre-neutectic crystallization of $\beta-Al_5FeSi$ - $T_{E(Fe)}$ phase.
 - Stage 3: dual eutectic crystallization of $\alpha(Al)+\beta(Si)$.
 - Further crystallization stages unchanged.
- for contents of more than 0.9wt.% Fe:
 - Stage 1: nucleation and primary crystallization of the phase $\beta-Al_5FeSi$ - $T_{E(Fe)}$.
 - Stage 2: crystallization of solid solution dendrites $\alpha(Al)$ - $T_{\alpha(Al)}$.
 - Stage 3: crystallization of the double eutectic $\alpha(Al)+\beta(Si)$ and further stages without change.

Based on microscopic studies, it can be concluded that in the AlSi7Mg alloy, there are dendrites of solid solution $\alpha(\text{Al})$, which constitute the matrix of the alloy, silicon crystals $\beta(\text{Si})$, which are part of the double eutectic $\alpha(\text{Al})+\beta(\text{Si})$, Mg_2Si phase - as a component of the eutectic $\alpha(\text{Al})+\text{Mg}_2\text{Si}+\beta(\text{Si})$, and separations of the $\beta\text{-Al}_5\text{FeSi}$ phase with lamellar morphology (on the surface of the needle-shaped deposit). Based on ATD, microstructure studies, and literature review [17, 20, 21], it was concluded that the essential criteria determining the formation of a particular type of iron phase include the alloy's iron content and its cooling rate. Phases that crystallize before the formation of the $\alpha(\text{Al})$ solid solution dendrites growing freely in the metallic liquid, or those that form at the same time as the dendritic network (but in the remaining liquid), tend to grow much more significantly ($\beta\text{-Fe}$ phase) than those that form later - during or after the formation of the $\alpha(\text{Al})+\beta(\text{Si})$ eutectic and the $\alpha(\text{Al})+\text{Mg}_2\text{Si}+\beta(\text{Si})$ triple eutectic. The increase in the size of the $\beta\text{-Al}_5\text{FeSi}$ phase, due to the rise in the iron content of the AlSi7Mg alloy, also directly correlates with its silicon concentration. According to research results [20, 21], there is a close correlation between the silicon content and the resulting iron content, which may be acceptable before crystallization (mainly primary crystallization) of the $\beta\text{-Al}_5\text{FeSi}$ phases begins. The iron level is referred to as the so-called "critical" level and follows the relationship [21]:

$$Fe_{kryt} = 0.075 \cdot (\text{wt. \% Fe}) - 0.05 \quad (1)$$

According to this relationship, the Fe_{kryt} for Al-Si alloys with about 7 wt. % Si is about 0.47 wt. % Fe, which is consistent with the results of ATD and microstructure studies of AlSi7Mg alloy presented here. The consequence of neutralizing the morphologically and dimensionally unfavorable $\beta\text{-Al}_5\text{FeSi}$ phases in Al-Si alloys is the introduction of elements that, due to their physicochemical properties, tend to change the unfavorable form of iron phases. Studies [18, 19, 22-27] show that manganese, chromium, and cobalt are additives. Research into the effects of these elements on the crystallization of iron phases, microstructure, and properties of Al-Si alloys is ongoing.

Based on the study, the following conclusions were made:

1. In AlSi7Mg alloy with content up to about 0.45wt.% Fe, crystallizing iron phases are included in multicomponent eutectics with little effect on the microstructure.
2. The content of about 0.5 to about 0.9wt.%Fe causes a change in the crystallization order of the AlSi7Mg alloy. The $\beta\text{-Al}_5\text{FeSi}$ phase separations crystallize before the eutectic $\alpha(\text{Al})+\beta(\text{Si})$, in the temperature range from about 574 to about 590°C. Their average length ranges from about 500 μm to 600 μm .
3. At a content of more than 0.9wt.% Fe, the $\beta\text{-Al}_5\text{FeSi}$ phases crystallize initially in the temperature range from about 590 to as much as 640°C. Their average length ranges from 600 μm to 1000 μm . The free-growing lamellar-ligneous $\beta\text{-Fe}$ phases block interdendritic channels and impede liquid melt flow, causing increased casting porosity.

5. References

1. Brown M.E.: Introduction to thermal analysis techniques and applications, New York, Kluwer Academic Publishers, 2004.
2. Djurdjevic M.B., I. Vicario, G. Huber: Present and Future Application of the Thermal Analysis in Aluminum Casting Industry, *Revista de Metalurgia*, 50(1), 2014, 1-12.
3. Emadi D., L.V. Whiting, S. Nafisi, R. Ghomashchi: Thermal analysis applications in quality control of solidification processes, *Journal of Thermal Analysis and Calorimetric*, 81(1), 2005, 235-242.
4. A.J. Ryan: Thermogravimetric Analysis (TGA). Theory and Applications.
5. Saadatkhani N., A.C. Garcia, S. Ackermann, P. Leclerc, M. Latifi, S. Samih, G.S. Patience, J. Chaouki: Experimental methods in chemical engineering: Thermogravimetric analysis-TGA, *The Canadian Journal of Chemical Engineering*, 98, 2020, 34-43.
6. Gol A.O.K.: Quantification of phase transformations using calorimetry and dilatometry, Alberta, University of Alberta, 2015.
7. Chen G., S. Zhang, Y. Zhu, C. Yang, Q. Shi: Thermo-mechanical Analysis of Friction Stir Welding: A Review on Recent Advances, *Acta Metallurgica Sinica*, 33, 2020, 3-12.
8. Spink C.H.: Differential Scanning Calorimetry, *Methods in Cell Biology*, 84, 2008, 115-141.
9. Menczel J.D., R.B. Prime: Thermal analysis of polymers. Fundamentals and Applications, New Jersey, A John Wiley and Sons, 2009.
10. Tarasom A.: Thermal analysis: methods, principles, application. Lecture series, 2012.
11. Gabbott P.: Principles and Applications of Thermal Analysis, Hoboken, Blackwell Publishing Ltd, 2008.
12. Bouzidi L., M. Boodhoo, K.L. Humphrey, S.S. Narine: Use of first and second derivatives to accurately determine key parameters of DSC thermographs in lipid crystallization studies, *Thermochimica Acta*, 439(1-2), 2005, 94-102.
13. Djurdjevic M.B.: Application of thermal analysis in ferrous and nonferrous foundries, *Metallurgical and Materials Engineering*, 27, 2021, 457-471.
14. Erbaş K.C.: A new baseline for the Newtonian thermal analysis of casting: two-capacitive system baseline: modeling the effects of the thermal capacity of mold, *Journal of Thermal Analysis and Calorimetry*, 119(1), 2014, 183-189.
15. Piątkowski J., B. Gajdzik: Testing phase changes in Al-Si alloys with application of thermal analysis and differential calorimetric analysis, *Metallurgija*, 52, 2013, 469-472.
16. Zakharchenko E., E. Sirenko, A. Goncharov, A. Bogdan, A. Burbelko, M. Kawalec: New Computer Method of Derivative Thermal Express Analysis of Cast Iron for Operational Prediction of Quality of Melts and Castings, *Journal of Casting & Materials Engineering*, 3, 2019, 31-42.
17. Xinjin C., J. Campbell: Morphology of $\square\text{-Al}_5\text{FeSi}$ phase in Al-Si cast alloys, *Materials Transaction*, 47, 2006, 1303-1312.
18. Moustafa M.A.: Effect of iron content on the formation of $\beta\text{-Al}_5\text{FeSi}$ and porosity in Al-Si eutectic alloys, *Journal of Materials Processing Technology*, 209, 2009, 605-610.
19. Piątkowski J., S. Roskosz, S. Stach: The Influence of Selected High - Pressure Die Casting Parameters on the Porosity of ENAB-46000 Alloy Castings, *Advances in Science and Technology* 18(5), 2024, 361-371.
20. Taylor J.A.: The effect of iron in Al-Si cast alloys, *ResearchGate*, 2004. 1-12.
21. Taylor, J.A.: Iron-containing intermetallic phases in Al-Si based casting alloys, *Procedia Materials Sci.*, 1, 2012, 19-33.
22. Ferraro S., A. Fabrizi, G. Timelli: Evolution of sludge particles in secondary die-cast aluminium alloys as function of Fe, Mn and Cr contents, *Materials Chemistry and Physics*, 153, 2015, 168-179.
23. Ceschini L., I. Boromei, A. Morri, S. Seifeddine, I. Svensson: Microstructure, tensile and fatigue properties of the Al-10% Si-2% Cu alloy with different Fe and Mn content cast under controlled conditions, *Journal of Materials Processing Technology*, 209, 2009, 5669-5679.
24. Piątkowski J., M. Hejne, R. Wieszala: Influence of manganese content on the microstructure and properties of AlSi10MnMg(Fe) alloy for die castings, *Archives of Materials Science and Engineering*, 123, 2023, 5-12.
25. Seifeddine S., I.L. Svensson: The influence of Fe and Mn content and cooling rate on the microstructure and mechanical properties of A380-die casting alloys, *Metallurgical Science and Technology*, 27, 2009, 11-20.
26. Shabestari S.G.: The Effect of iron and manganese on the formation of intermetallic compounds in Al-Si alloys, *Materials Science and Engineering A*, 383, 2004, 289-298.
27. Mahta M., M. Emamy, A. Daman, A. Keyvani, J. Campbell: Precipitation of Fe-rich intermetallics in Cr and Co modified A413 alloy, *International Journal of Cast Metals Research* 18, 2005, 73-79.